Bioelectrochemistry 149 (2023) 108312

Contents lists available at ScienceDirect

Bioelectrochemistry

journal homepage: www.journals.elsevier.com/bioelectrochemistry

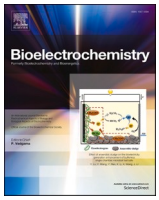

A label-free impedance-based electrochemical sensor based on self-assembled dendritic DNA nanostructures for Pb^{2+} detection

Huali Jin [a,*], Jie Dong [a], Xinru Qi [a], Xiaoxia Sun [b], Min Wei [a], Baoshan He [a], Zhiguang Suo [a,*]

[a] College of Food Science and Technology, Henan Key Laboratory of Cereal and Oil Food Safety Inspection and Control, Henan University of Technology, Zhengzhou 450001, China
[b] Henan Institute of Product Quality Supervision and Inspection, Zhengzhou 450002, China

ARTICLE INFO

Keywords:
Impedance-based electrochemical sensor
Gold nanomaterials
Hybridization chain reaction (HCR)
DNA self-assembly
Lead ion

ABSTRACT

Here, a label-free impedance-based electrochemical sensor was developed for the quantitative detection of Pb^{2+}. Using conductive gold nanomaterials as electrode substrate materials can provide sensors with larger specific surface area, action sites and excellent conductivity. DNA nanostructures are used for the determination of biomolecules due to their good properties. The Y-DNA structure is formed by the annealing of three DNA sequences, which acts as a stable structure and forms a dendritic structure in combination with the hybrid chain reaction. In the presence of the target Pb^{2+}, it induces the conversion of specific aptamers into G-quadruplexes, resulting in HCR and Y-DNA loading on the electrodes and a significant change in the impedance value signal. Therefore, the proposed biosensor realizes the quantitative detection of Pb^{2+}. Under the optimal experimental conditions, the concentration of Pb^{2+} exhibited a linear correlation range from 0.5 to1000 nmol/L with a limit of detection (LOD) of 0.38 nmol/L. The designed sensors have good recoveries in real samples (tap water and tea). This flexible experimental protocol has broad application prospects.

1. Introduction

As one of the three most toxic heavy metal pollutants in the environment and food, lead has the advantages of low melting point, high corrosion resistance, not being easily penetrated by X-rays and γ-rays, and good plasticity [1]. Based on these, lead elements are introduced into some materials (sheets, plates), which are widely used in chemical, cable, battery, radiation protection and other industrial sectors [2]. Therefore, lead exists in the environment in the form of ions or compounds, resulting in severe pollution of the atmosphere, soil and water sources [3]. As a non-essential element for the human body, lead is mostly brought into the human body through ingestion of food and drinking tap water. The lead that enters the human body cannot be metabolized and biodegraded, 90 % is stored in the bones, and 10 % is distributed to various tissues [4–6]. Lead is highly toxic, and acute poisoning can cause headaches, hallucinations, abdominal pain, osteoarthritis, and high blood pressure [7]. Chronic poisoning from long-term exposure to low levels of lead can lead to muscle weakness, congenital deformities and even death [8,9]. Especially after infants and young children absorb lead, more than 30 % of lead will remain in the body, which will cause irreversible effects on health and intelligence [10]. Therefore, heavy metal pollution research has become a hot issue in the field of public health. GB 5749–2006 stipulates that the maximum allowable level of lead in drinking water for residents is 0.01 mg/L (48.26 nmol/L) [11], GB 2762–2017 lists the lead limit value of various foods in detail, of which the limit standard for tea is 5.0 mg/kg [12]. The lead content in food is generally at the trace level. Therefore, establishing a lead detection method with high sensitivity, simple operation, rapid response and strong specificity is one of the important means to prevent the harm of heavy metal pollution.

Generally, heavy metal elements coexist in food and environment, the detection of Pb^{2+} may interfere with other metal ions [13]. Cai *et al.* [14] developed a detection method based on the FRET effect of Fe_3O_4@Au-FITC nanocomposites, Fe_3O_4@AuNPs-FITC can be etched by Pb^{2+} in the presence of $Na_2S_2O_3$, in which Hg^{2+}, Cu^{2+} and Ca^{2+} all interfere with Pb^{2+} at the same ion concentration detection. It is worth noting that the emergence of artificial aptamers as effective alternatives to antibodies provides more possibilities for constructing biosensors. An aptamer is an oligonucleotide sequence obtained by SELEX technology with high affinity and specificity, which can bind to a target to form a specific three-dimensional (3D) structure [15]. The synthesis and modification of aptamers are simple, the performance is stable, the

* Corresponding authors.
E-mail addresses: jinhuali66@163.com (H. Jin), zg_suo@163.com (Z. Suo).

https://doi.org/10.1016/j.bioelechem.2022.108312
Received 13 July 2022; Received in revised form 12 September 2022; Accepted 17 October 2022
Available online 21 October 2022

application is wide, the cost is low, and the biocompatibility is good. [16] Among aptamer-based sensors, electrochemical aptamer sensors have become widely used for the detection of pollutants such as heavy metal ions due to their fast response and low price. Electrochemical aptamer sensors are classified into label-free and label-based types according to whether the signal is from a redox label. Redox-labeled electrochemical aptamers have high sensitivity, however, the complex structure and high cost limit their development [17]. Therefore, the development of label-free electrochemical sensors can solve the above problems.

Meanwhile, nanomaterials, including gold nanoparticles, graphene oxide, and composite nanomaterials, have been widely introduced into the design of sensors due to their good biocompatibility, large specific surface area, good electrical conductivity, and ease of modification and synthesis. [18–20] Wang *et al.* [21] reported an aptamer for Pb^{2+} detection based on Au NPs-induced FRET with a detection limit of 4.1 nmol/L. However, contaminants in food are often present in trace amounts, so it is necessary to further improve the sensitivity of detection methods. He *et al.* [22] fabricated an electrochemical aptamer using polyethyleneimine-based graphitic carbonitride/gold nanowire composites (PEI-C_3N_4/AuNWs) as a signal amplification strategy. PEI-C_3N_4/AuNWs were modified on the surface of gold electrodes for the first time and exhibited good electrocatalytic performance, which could improve the electrical conductivity and specific surface area of gold electrodes. These results suggest that gold nanomaterials have ideal electrical conductivity and can be applied in electrochemical sensors to improve detection sensitivity. Compared with nanoparticles, the surface of nanoflowers is more wrinkled, so the adsorption sites are abundant. Therefore, simple preparation, high colloidal stability and nanoflowers have attracted extensive research interest. [23] Cui *et al.* [24] constructed a disposable-scale electrochemical adapter using in situ growth of gold nanoflowers (AuNFs) on indium tin oxide (ITO) surfaces to anchor methylene blue (MB)-labeled complementary DNA. The ferrocene (Fc)-labeled aptamer is then hybridized to cDNA (MB) to create a biphasic structure, resulting in a dual signal. The aptamer has a wide detection range of 0.1–1000 pg/mL and a low detection limit of 0.032 pg/mL.

Among the different types of DNA nanostructures, dendrimer DNA nanostructures are known for their high loadings, excellent biostability, and biocompatibility. [25] Dai *et al.* [26] 's new method for designing one-dimensional DNA polymer chains based on the self-assembly of CHA and sticky ends has been successfully used for AuNP-based colorimetric DNA detection, however, this strategy is time-consuming and costly. The sticky-tailed Y-DNA (Y-DNA), as the most commonly used monomer, is synthesized by the annealing of three single-stranded DNA (ssDNA) and does not require induction by other DNA strands. [27] Therefore, a facile, low-cost assembled and more complex DNA nanostructure can be developed based on Y-DNA monomers.

In order to enhance the sensitivity of the sensor detection process, various signal amplification methods have been introduced into the preparation of the sensor, such as hybridization chain reaction (HCR), rolling circle amplification (RCA), etc. [28,29] While hybridization chain reaction (HCR) relies only on the hybridization of two DNA strands without enzymatic catalysis, it is a very efficient signal amplification method, which can be used in the preparation of many sensors and can also be used in combination with other signal amplification strategies. [30] Yi *et al.* [31] prepared a novel label-free electrochemical aptamer sensor based on three-dimensional porous materials to detect acetamiprid residues. The prepared 3D-CS/rGO was modified on the electrode and the aptamer chain was immobilized and the hybridization chain reaction occurred. The addition of sodium molybdate can react with the phosphate groups of long DNA. The sensor has a wide linear range of 0.1 pmol/L – 0.1 μmol/L and a low detection limit of 71.2 fmol/L. Jiang *et al.* [32] modified the traditional linear HCR and developed a new bilinear hybridization chain reaction (DL-HCR) for DNA detection, which greatly amplified the electrochemical signal. Under optimized conditions, the sensor has a linear range of 20 fmol/L to 5 nmol/L. with a detection limit of 8.74 fmol/L. Therefore, the HCR amplification method holds great promise for economical, reliable, and high-sensitivity gene sensing applications.

Inspired by these studies, an impedance electrochemistry aptamer sensor was constructed for the detection of Pb^{2+} by an ingenious combination of gold nanomaterials and dendrimer DNA nanostructures. In this work, Au NFs with larger specific surface area and higher conductivity were prepared, and the hybrid chain reaction and DNA self-assembly were cleverly combined for the first time. In the presence of Pb^{2+}, the cDNA loaded on the electrode completes the hybridization chain reaction with the added DNA strand through base complementary pairing, and assembles on the electrode to form a dendritic structure, generating a signal to detect metal ions.

2. Experimental sections

2.1. Materials

All oligonucleotide sequences used in the experiments were synthesized, modified and purified in Sangon Biotechnology Co., ltd (Shanghai, China). Detail sequences are given in **Table S1**. $K_4[Fe(CN)_6]\cdot 3H_2O$ (99.5 %) and KCl (99.5 %) were purchased from Tianjin Regent Chemical Co., ltd, $Na_2HPO_4\cdot$(99.0 %), NaCl (99.5 %), KH_2PO_4 (99.5 %), Pb $(NO_3)_2$ (99.0 %) and $C_6H_6O_2$ (99.0 %) were purchased from Tianjin Komiou Chemical Regent Co., ltd, K_3[Fe $(CN)_6$] (99.5 %) were purchased from Shanghai West Asia Chemical Industry and Trade Co., ltd, TCEP (99.5 %) were purchased from Shanghai Yuanye Biological Technology Co., ltd, C_2H_6O (99.7 %) were purchased from Tianjin TianliChemical Regent Co., ltd, $HAuCl_4\cdot 4H_2O$ (99.9 %) were purchased from Tianjin Chemical Reagent Co., ltd and $C_6H_5O_7Na_3\cdot 2H_2O$ (99.5 %) were purchased from Luoyang Haohua Chemical Reagent Co., ltd. The other main materials and chemical reagents used in this experiment are of analytical grade (purity of 99.0 %); the water used in this experiment is sterilized ultrapure water (resistivity, 18.25 MΩ). All oligonucleotides were diluted with 20 mmol/L Tris-HCl buffer, and all reagents shall be fully mixed before use.

2.2. Instrument

A traditional three-electrode system was used in this experiment, which mainly includes a working electrode (AuE, diameter of 3 mm), reference electrode and counter electrode. The parameters of the electrochemical impedance spectroscopy (EIS) were set as: the potential is 0.19 V, the scan rate is 5 mV/s, the scan range is 0.1 to 10 kHz, detected in 5 mmol/L [Fe $(CN)_6$]$^{3-/4-}$ solution (containing 0.5 mol/L KCl). All electrochemical behaviors were performed on a CHI-660E electrochemical workstation (Shanghai Chenhua Instrument Co., ltd., China). Transmission electron microscopy (TEM, JEM-100SX Japan), Scanning electron microscopic (SEM, JSM-7610F, Japan) and, X-ray diffraction (XRD, Bruker D8 Advance, Germany), Zeta potential (Zeta, nano ZS, U. K.) and "Nano-Measurer 1.2″ software were used for the characterization of nanomaterials.

2.3. The preparation of Au NFs

According to the reported method, Au NFs were synthesized by the seed-mediated growth method using $HAuCl_4$ as the precursor and growth solution and $C_6H_5O_7Na_3$ $2H_2O$ as the reducing agent. [33] First, colloidal gold nanoseeds (Au NSs) were prepared by a classical hydrothermal reduction method. Briefly, 1 mL of $HAuCl_4$ (1 %) and 99 mL of ultrapure water were mixed and heated until the mixture boiled. 2.7 mL of $C_6H_5O_7Na_3$ $2H_2O$ (1 %) was quickly added to the boiling solution and continued to boil for 10 min until a clear wine-red solution was formed, indicating that Au NSs were successfully prepared. Then, gold nanoflowers with dandelion-like surfaces were prepared by a seed-mediated

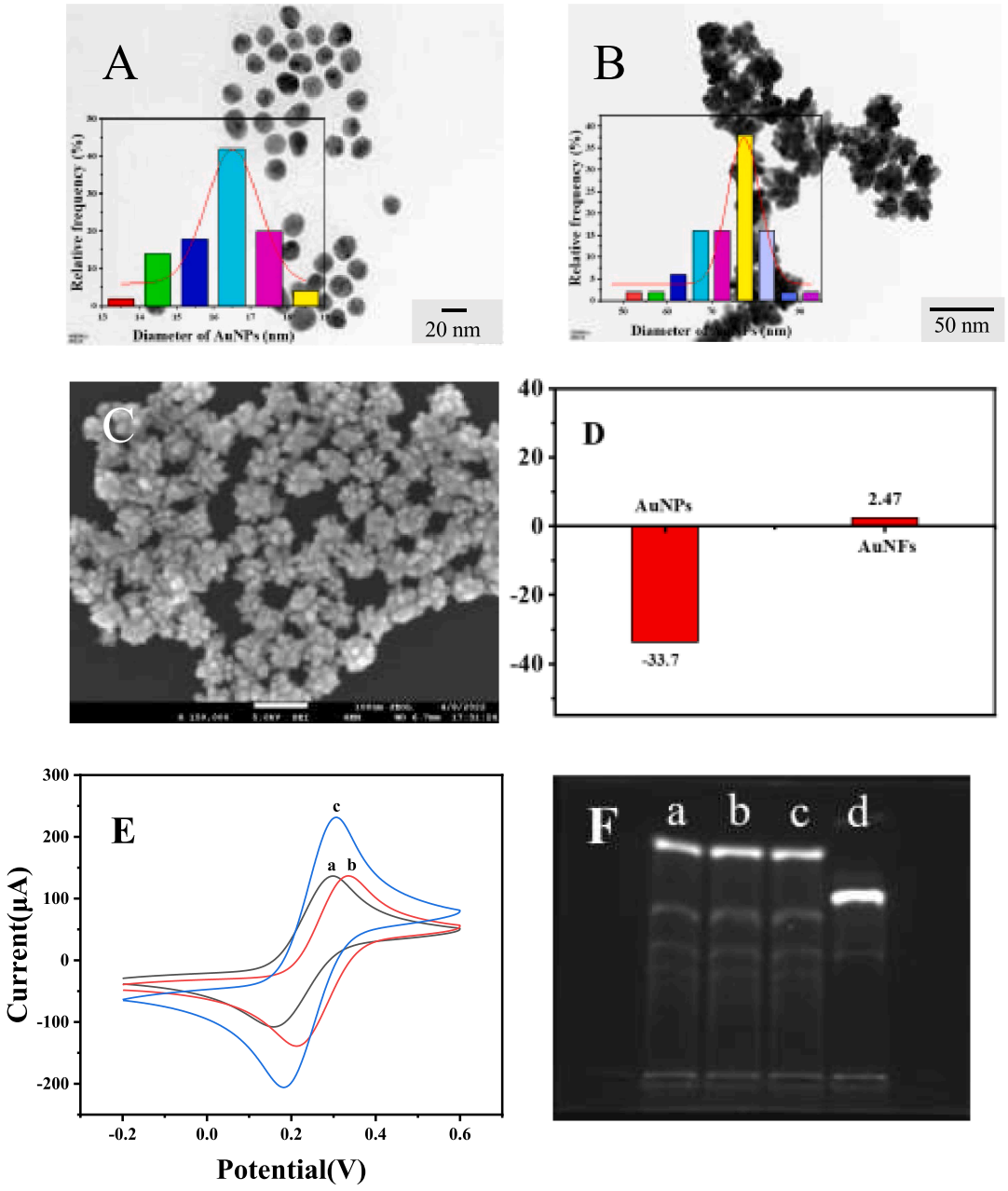

Fig. 1. (A) TEM diagram of Au NPs, inset: histogram and normal distribution curve of Au NPs particle size distribution. (about 16 nm); (B) TEM diagram of Au NFs, inset: histogram and normal distribution curve of Au NFs particle size distribution. (about 75 nm); (C) SEM diagram of Au NFs; (D) Zeta of Au NPs and Au NFs; (E) CV of Au NPs and Au NFs modified on the AuE. (F) Agarose gel electrophoresis: (a) m, (b) n, (c) q, (d) Y-DNA.

growth method. Under vigorous stirring, 375 μL $HAuCl_4$ (1 %), 220 μL $C_6H_5O_7Na_3$ $2H_2O$ (1 %), and 1.78 mL Au NSs were sequentially added to 100 mL ultrapure water. Then 1 mL of 30 mmol/L 1,4-hydroquinone was added to the mixture and stirring was continued for 30 min at 25 °C. The synthesized transparent dark blue Au NFs solution was centrifuged at 8000 r/min for 15 min, washed three times with ultrapure water, and finally concentrated in ultrapure water to obtain a suspension with a concentration of 3600 pmol/L. The reactions were all carried out with vigorous stirring.

2.4. The construction of the sensor

The construction of Y-DNA nanostructure: ssDNA m, n, q (final concentrations 2.0, 1.0 and 1.0 μmol/L) in Y-DNA were mixed by vortexing to form DNA strand complexes, then kept at 95 °C in the PCR machine for 5 min, and then slowly cooled. The cooling rate was controlled at 1 °C/min to allow annealing to form the Y-DNA structure. 100 μmol/L thiol-modified cDNA was heated at 95 °C for 10 min, and then slowly cooled to room temperature. It was put into a PBS buffer solution containing 10 mmol/L TCEP and incubated in the dark for 1 h to cleave the disulfide bonds.

First, 5 μL of AuNFs was added dropwise to the surface of the dry gold electrode, incubated in a constant temperature and humidity chamber at 37 °C for 2 h, and the electrode was taken out and washed three times with PBS buffer. The above-treated cDNA (5 μL, 2 μmol/L) was dropped on the surface of the gold electrode and incubated in a constant temperature and humidity chamber at 37 °C for 2 h. After washing the electrode, MCH (5 μL, 1 mmol/L) was added to the electrode surface and incubated for 1 h to occupy the excess sites on the electrode surface. 5 μL of mixed solutions containing Apt and different concentrations of Pb^{2+}

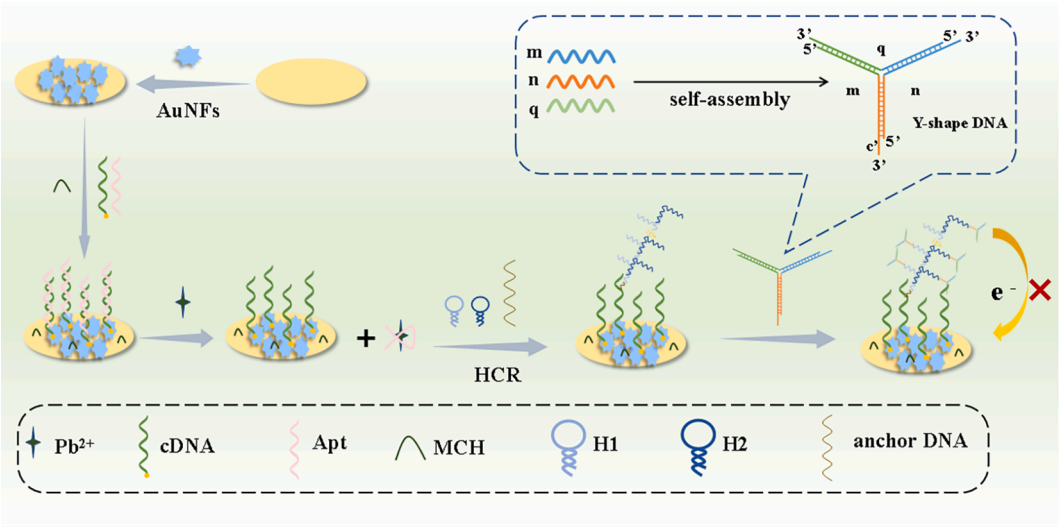

Scheme 1. Schematic diagram on the fabrication of Y-DNA/H1H2/anchor DNA/Apt-Pb^{2+}/MCH/cDNA/AuNFs/AuE sensor and mechanism of Pb^{2+} detection.

(the final concentration of Apt is 2 μmol/L) was added dropwise to the electrode surface, and incubated at 37 °C for 2 h. Finally, the mixed solution of anchor DNA, H1H2 and Y-DNA was added dropwise to the electrode surface and incubated at 37 °C for 1.5 h to obtain the sensor of this experiment. After rinsing the electrodes, it was placed in 5 mmol/L $[Fe(CN)_6)]^{3-/4-}$ solution (containing 0.5 mol/L KCl) for EIS measurement.

2.5. Detection of Pb^{2+}

5 μL of cDNA mixed solution was dropped on the surface of the gold nanoflowers-modified electrode, and incubated in a constant temperature and humidity chamber at 37 °C for 2 h. After rinsing the electrode, add MCH (5 μL, 1 mmol/L) on the electrode surface and incubate for 1 h. Then, 5 μL of Pb^{2+} (50 nmol/L) solution and 5 μL of blank solution were respectively added to the surface of MCH/cDNA/AuE and incubated for 30 min. Finally, anchor DNA, H1H2 and Y-DNA were dropped on the electrode surface and incubated for 90 min. Then, it was placed in 5 mmol/L $[Fe(CN)_6)]^{3-/4-}$ solution (containing 0.5 mol/L KCl) for EIS measurement. The sensor is used to detect Pb^{2+} according to the difference in impedance value.

2.6. Detection of actual samples

In order to study the detection performance of the aptamer sensor in real samples, the spiked recovery experiments were carried out on tap water (from Lianhu of Henan university of technology) and tea. The tap water was not pretreated, and the pretreatment procedure for tea was improved on the basis of the published literature. [34] The recovery rate was calculated based on three times data.

Tea samples: take dried tea leaves, grind finely, sieve and remove stems. Accurately weigh 5 g of tea powder, dissolve it in 100 mL of ultrapure water, and extract in a 90 °C water bath at a constant speed of 600 r/min for 30 min. The extract was cooled to room temperature with stirring, centrifuged at 9000 r/min for 15 min, and then a 10 mL volume of filtrate was obtained using a 0.45 μm diameter syringe filter. Then, the tap water samples and tea filtrate were mixed with Pb^{2+} standard solution (diluted 10-fold and 100-fold, respectively), and spiked recovery experiments were performed. The final Pb^{2+} concentrations were 0.5, 10, and 100 nmol/L, respectively.

3. Results and discussion

3.1. The structural characteristics of Au NFs and DNA nanostructures

According to the synthesis method reported in reference, a series of operations were performed to obtain Au NFs materials. [35] Fig. 1**A** shows the TEM of Au NPs, clearly granular (10 to 20 nm in diameter), and the crystalline AuNPs were characterized by XRD in **Fig. S1**, and the diffraction peaks of the (1 1 1) showed that the prepared gold nanoparticles were relatively pure. The Fig. 1**B** shows the TEM of Au NFs, where dandelion-like gold nanoflowers can be clearly seen. Au NFs have a larger surface area (60 to 80 nm in diameter) with more attachment sites, allowing more DNA strands to be immobilized. As shown in Fig. 1**C**, we can also observe the morphology of gold nanoflowers by SEM, these results all demonstrate the successful preparation of AuNFs. As shown in Fig. 1**D,** we tested the zeta potential. And it can be seen that the prepared gold nanoparticles have more negative charges, and the gold nanoflowers have positive charges. Since the phosphate backbone of our DNA chain is negatively charged, the electrostatic adsorption between gold nanoflowers and DNA chains will be higher than that of gold nanoparticles. Therefore, we used gold nanoflowers as the electrode substrate material in our experiments.

At the same time, we also compared the electrical conductivity of the two materials through the CV. As shown in Fig. 1**E**, the peak current value of the Au NFs modified electrode (c) was significantly increased by 2 times (from 158 μA to 259 μA) compared with the Au NPs modified electrode (b), indicating that the Au NFSs were more conductive. According to equation (1), the actual electrode surface was measured.

$$Ip = (2.69 \times 10^5)\, AD^{1/2}n^{3/2}\upsilon^{1/2}C \quad (1)$$

where A is the electroactive surface area (cm^2), D is the diffusion coefficient (cm^2/s), n is the number of electrons transferred, υ is the scan rate (υ/s), and C is the redox volume concentration probe (mol/cm^3). The specific surface area of the Au NFs modified electrode (0.2354 cm^2) is about 2 times that of the Au NPs modified electrode (0.1436 cm^2).

The agarose gel electrophoresis was used to verify whether the DNA nanostructures can be assembled successfully. As shown in Fig. 1**F,** m, n and q show nearly identical mobilities (lanes a-c), indicating that m, n and q have the same number of bases. This result is consistent with our design. It is important to confirm whether the hybridization reaction between m, n and q forms a Y-DNA structure. When the three strands were incubated together, a lower mobility streak was observed (lane d), indicating that the Y-DNA was successfully assembled.

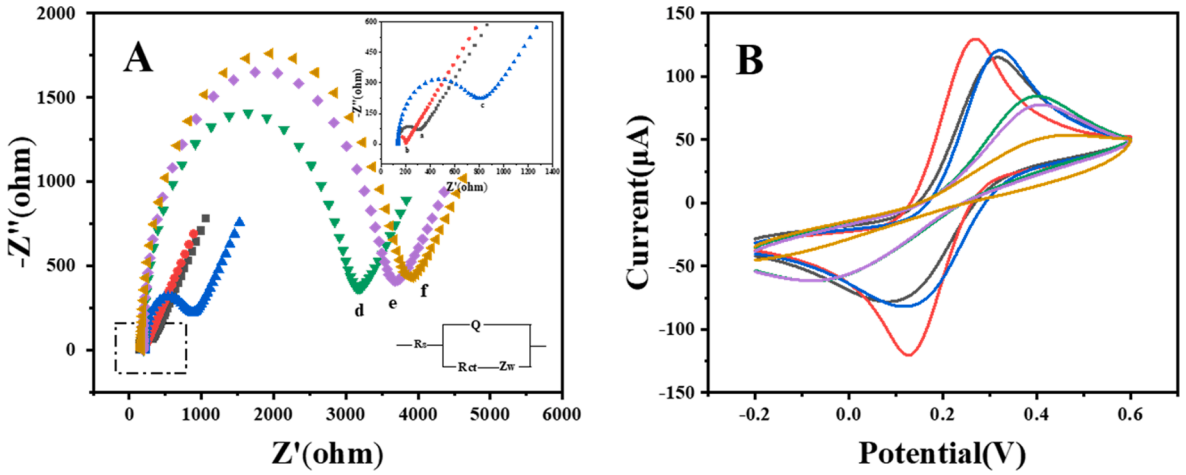

Fig. 2. (A) EIS of different modified electrodes in 5 mmol/L $[Fe(CN)_6]^{3-/4-}$ (containing 0.1 mol/L KCl) solution. (a) AuE; (b) AuNFs/AuE; (c) cDNA/AuNFs/AuE; (d) MCH/cDNA/AuNFs/AuE; (e) Apt-Pb^{2+}/MCH/cDNA/ AuNFs/AuE; (f) Y-DNA/H1H2/anchor DNA/Apt-Pb^{2+}/MCH/cDNA/AuNFs/AuE (B) CV curves at various modification steps of the electrode. AuE (black curve); AuNFs/AuE (red curve); cDNA/AuNFs/AuE (blue curve); MCH/cDNA/AuNFs/AuE (red curve); Apt-Pb^{2+}/ MCH/cDNA/ AuNFs/AuE (green curve); Y-DNA/H1H2/anchor DNA/Apt-Pb^{2+}/MCH/cDNA/AuNFs/AuE (yellow curve).

3.2. Detection principle of electrochemical aptamer sensor

Based on the electrical conductivity of gold nanomaterials and dendritic DNA nanostructures as a signal amplification strategy, an impedance-type electrochemical aptamer was constructed for the detection of Pb^{2+}. The detection principle is shown in Scheme 1. The Y-DNA structure is formed in which three ssDNAs (m, n, q) hybridize pairwise by base complementation. First, the cDNA with modified thiol group at the 5′ end was immobilized on the surface of AuE modified by gold nanomaterials through Au-S bonds, and the unbound sites were blocked with MCH to avoid non-specific adsorption. In the absence of Pb^{2+}, the added Apt forms a double-stranded structure with cDNA through base complementary pairing. The anchor DNA cannot open the double-stranded structure, and the subsequent anchor DNA, H1H2 and Y-DNA structures cannot bind to the electrode surface. At this time, there is less DNA phosphate backbone on the electrode, which is beneficial for $[Fe(CN)_6]^{3-/4-}$ to reach the electrode surface for redox, resulting in a smaller impedance value. In the presence of Pb^{2+}, due to the strong binding ability of Pb^{2+} and Apt, a heavy metal-aptamer complex was formed, which fell off the electrode surface after being washed with PBS buffer. The remaining cDNA on the electrode surface can carry out a hybridization chain reaction with anchor DNA, H1H2 and Y-DNA structure, and the dendritic DNA nanostructure is formed on the electrode. At this time, there are many DNA phosphate skeletons on the electrode, which is not conducive to $[Fe(CN)_6]^{3-/4-}$ reaching the electrode surface for redox, resulting in a larger impedance value. Therefore, the detection of Pb^{2+} can be realized by the difference in impedance value with or without Pb^{2+}.

3.3. Electrochemical behavior of the designed electrochemical sensor

The fabrication successfully and functioning well of this biosensor was investigated and validated by CV and EIS methods. [36–38] EIS of different modified electrodes in 5 mmol/L the $[Fe(CN)_6]^{3-/4-}$ (containing 0.5 mol/L KCl) solution. As shown in Fig. 2**A**, the impedance of the bare AuE is small (a) at 149.3 Ω, which is due to the high electron transfer efficiency of the bare electrode, indicating that the gold electrode is well treated. After the gold nanoflowers were modified on the electrode surface, the impedance value dropped to 68.74 (b), indicating that the gold nanoflowers had better conductivity and improved the electron transfer rate. After the cDNA was immobilized on the modified electrode surface, the impedance suddenly increased to a large value of 581.5 Ω (c), which was because the phosphate backbone of the negatively charged cDNA interacted with the negatively charged $[Fe(CN)_6]^{3-/4-}$ repel each other, hindering electron transfer on the electrode surface. The unbound site is blocked by MCH and the impedance value increases to 2769 Ω (d). Apt and Pb^{2+} were dropped on the electrode surface. Since the binding ability of Apt and Pb^{2+} was greater than the ability of Apt to pair with cDNA bases to form double strands, Apt-Pb^{2+} complexes were formed and fell off the electrode surface, and the impedance value was 3256 Ω (e). The addition of Anchor DNA makes a small amount of Apt not bound to Pb^{2+} form a double-stranded structure with cDNA. With the addition of H1H2 and Y-DNA, more and more negatively charged DNA strands are immobilized on the electrode due to the hybridization chain reaction, preventing $[Fe(CN)_6]^{3-/4-}$ from reaching the electrode surface, so the impedance value increases to 3466 Ω (f).

In addition, the differences in electrochemical activities throughout the structure characterization and detection process of the modified electrode were analyzed using CV (Fig. 2**B**). Au NFs are deposited onto bare gold electrodes (black curve) by physical adsorption, and the current increases sharply (red curve). The existence of the negatively charged phosphates in cDNA structure and its large size effectively hampered the electron transfer from $[Fe(CN)_6]^{3-/4-}$ as the negatively charged redox agent, leading to a significant reduction in the current signal (blue curve). Blocking the unbound site with MCH reduces the current signal (green curve). After the addition of target molecules (Pb^{2+}) on the Apt/ Pb^{2+} modified electrode surface, the electron transfer properties of the sensing interface were partially hindered (purple curve) due to the development of the Apt/ Pb^{2+} conjugate and its release on the electrode surface. Treatment of the electrodes with anchored DNA, H1H2 and Y-DNA resulted in another sharp drop in peak current (yellow curve), confirming the successful growth of dendritic DNA on the electrodes, reducing electron transfer.

3.4. Optimization of the experimental parameters

The ability of the sensor is significantly affected by the detection of experimental conditions. In order to obtain the best sensor performance, the effects of factors such as the concentration of cDNA, the concentrations of H1H2, and the concentration ratio of triplex in Y-DNA on the experimental results were investigated. The amount of cDNA immobilized on the electrode surface will affect the degree of hybridization chain reaction with H1H2, which will indirectly affect the impedance value of the sensor, which needs to be optimized. The aptamer sensor was constructed using 0.5–3.0 μmol/L cDNA. Fig. 3**A** shows that the

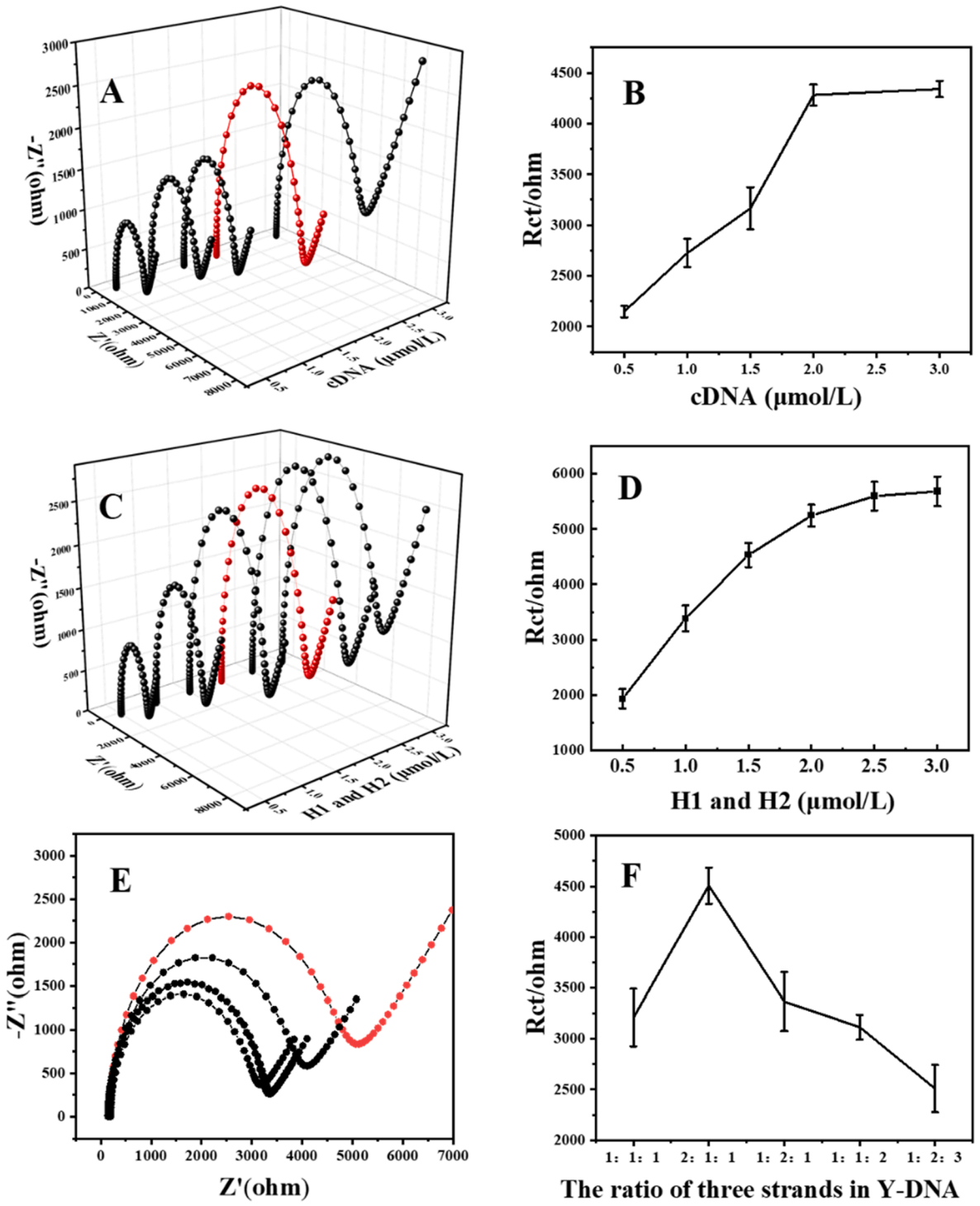

Fig. 3. Optimization of detection conditions: (A, B) the concerntration of cDNA (μmol/L); (C, D) the concerntration of H1H2 (μmol/L); and (E, F) the ratio of three strands in Y-DNA. The concentrations of Pb^{2+} were 500 nmol/L.

impedance value of the sensor increases significantly with the increase of the amount of cDNA added at the beginning, because more DNA strands can bind to the surface of Au NFs to participate in the construction of the sensor. The impedance value reached a maximum as the amount of cDNA increased to 2.0 μmol/L. Subsequently, the added resistance values of more cDNAs flattened. This is because the cDNA on the surface of Au NFs is saturated, and increasing the cDNA concentration has little effect on the experimental results. Therefore, 2.0 μmol/L cDNA was used in the construction of the aptamer.

The addition of HIH2 will cause the system to undergo a hybridization chain reaction, and more and more negatively charged DNA chains will be fixed on the electrode, preventing $[Fe(CN)_6]^{3-/4-}$ from reaching the electrode surface, and the impedance value will increase. But considering the cost, the concentrations of H1H2 were optimized. With the increase of H1H2 additions, the impedance value of the sensor increases rapidly. However, as the concentrations of H1H2 increased, the increase rate of the impedance value decreased and became stable, indicating that the hybridization chain reaction of H1H2 at this time (2 μmol/L) had the best effect (Fig. 3**C**). Therefore, H1H2 concentrations of 2.0 μmol/L were used in subsequent experiments.

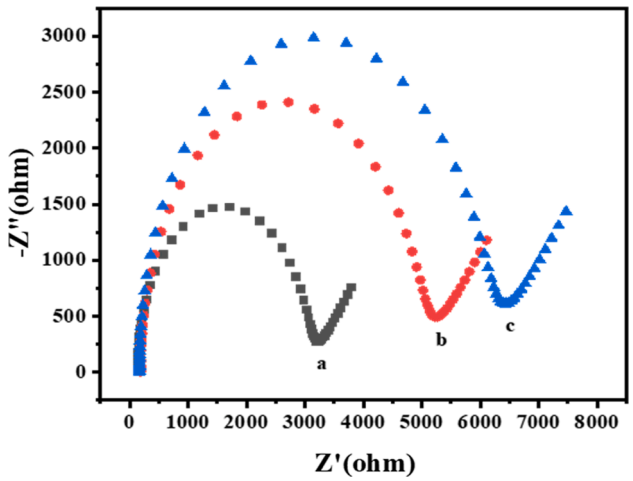

Fig. 4. Electrochemical Impedance Spectroscopy (EIS) curves at different situation (a) without Pb^{2+}; (b) with and Pb^{2+} containing 50 nmol/L; (c) with and Pb^{2+} containing 500 nmol/L in 5 mmol/L $[Fe(CN)_6]^{3-/4-}$ (with 0.1 mol/L KCl) solution.

The ratio of the three strands in Y-DNA will also have a direct impact on the performance of the sensor, so the ratio of the concentration of the three strands in Y-DNA is optimized. The experimental results are shown in Fig. 3**E**. The m: n: q concentration ratio is designed to be 2:1:1, and the impedance value of the sensor is as high as 4578 Ω, which is because the concentration of chain m in 2:1:1 is higher, which can be more connected to the hybridization chain reaction, hindering electron transfer, resulting in a larger impedance value. The ratios of the three chains of other designs are 1:1:1, 1:2:1, 1:1:2, 1:2:3, and the possibility of connecting to the electrode decreases due to the decrease in the concentration of chain m at this time, the impedance value is significantly reduced. Therefore, 2:1:1 was chosen as the optimal concentration ratio of the three chains in this experiment.

3.5. Feasibility analysis of the designed electrochemical sensor

In order to verify the feasibility of the prepared sensor, the impedance value is shown in Fig. 4 in the absence and presence of Pb^{2+}. In the absence of Pb^{2+} (a), the added Apt formed a double-stranded structure with the cDNA immobilized on the surface of the gold electrode, and the EIS value in 5 mmol/L $[Fe(CN)_6]^{3-/4-}$(containing 0.1 mol/L KCl) solution was 3108 Ω. After adding Pb^{2+} at a concentration of 50 nmol/L (b), the Apt-Pb^{2+} complex formed was washed away from the electrode by the PBS buffer because the binding capacity of Apt and Pb^{2+} was greater than the ability of Apt to base-pair with cDNA to form a duplex. The remaining cDNA on the electrode undergoes chain reaction with the subsequently added DNA strand, and the EIS value in 5 mmol/L $[Fe(CN)_6]^{3-/4-}$(containing 0.1 mol/L KCl) solution is 4702 Ω. After the addition of 500 nmol/L Pb^{2+} (c), the EIS value in 5 mmol/L $[Fe(CN)_6]^{3-/4-}$ (with 0.1 mol/L KCl) solution was 7575 Ω. Therefore, Pb^{2+} can be detected by the change of impedance value before and after adding Pb^{2+}.

3.6. Detection of Pb^{2+}

The performance of the prepared sensor was investigated by analyzing different concentrations of Pb^{2+} solutions under optimal experimental conditions (Fig. 5**A**). It can be clearly observed that in the range of 0.5–1000 nmol/L, with the increase of Pb^{2+} concentration, the impedance value gradually increases. An excellent linear relationship was obtained between the concentration of Pb^{2+} and the impedance value (Fig. 5**B**). The linear equation is $\Delta Rct = 583.2 + 671.11 LgCPb^{2+}$ (mol/L), the correlation coefficient is 0.992, and the detection limit is 0.38 nmol/L. We also calculated the LOQ according to the International Union of Pure and Applied Chemistry (IUPAC) to be 1.26 nmol/L.

These data all indicate that the electrochemical sensor has high sensitivity for the detection of Pb^{2+}.

3.7. Specificity, stability, repeatability, and reproducibility of impedance electrochemistry aptamer

To verify the selectivity of the aptamer for Pb^{2+}, a series of common metal interfering ions (K^+, Hg^{2+}, Cu^{2+}, Co^{2+}, Zn^{2+}, Mn^{2+}, Ba^{2+}, and Ni^{2+}) were tested using the same procedure used to detect Pb^{2+}. To evaluate the selectivity of the sensor for Pb^{2+}, the proposed measurement uses other common metal ions as interfering species, including K^+, Hg^{2+}, Cu^{2+}, Co^{2+}, Zn^{2+}, Mn^{2+}, Ba^{2+}, and Ni^{2+}. The results are shown in Fig. 6**A**, where the presence of interfering ions (100 times the concentration of Pb^{2+}) produced weaker impedance values. Furthermore, Pb^{2+} was still detected by the aptamer sensor even when all interfering ions coexisted with Pb^{2+}. These results demonstrate the excellent selectivity of the method even in the presence of a large number of interferents.

It is also important that the sensing device remains stable for extended periods of time under normal storage conditions (usually 4 °C). Therefore, the storage stability of this aptamer was tested. The

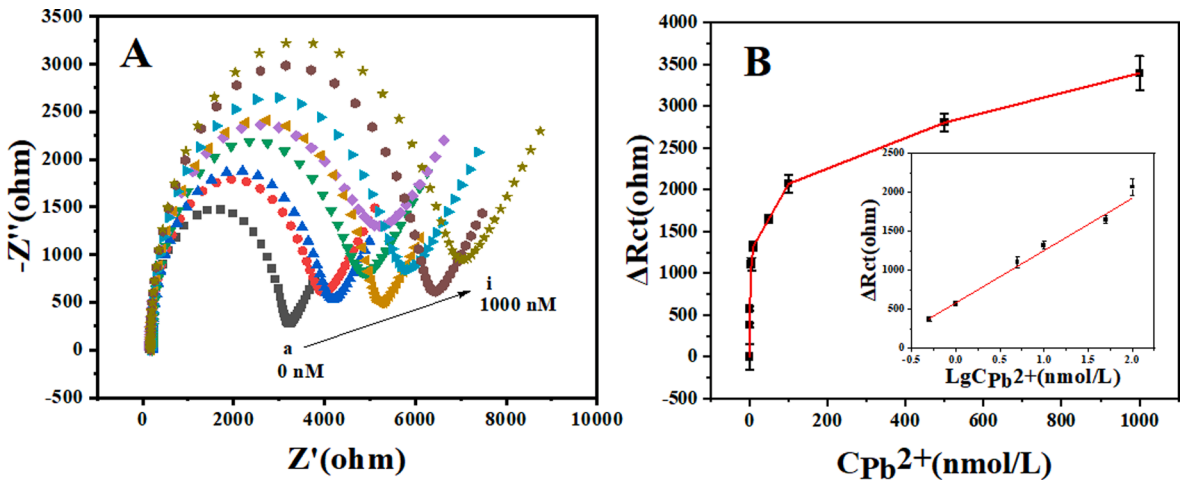

Fig. 5. (A) EIS curve in the range of 0 to 1000 nmol/L of Pb^{2+}:0, 0.5, 1,5, 10, 50, 100, 500 and 1000 nmol/L; (B) Relationship between Pb^{2+} concentration and relative impedance value in the range of 0–1000 nmol/L. Inset: the linear relationship between the concentration of Pb^{2+} and the relative impedance value in the range of 0.5–1000 nmol/L. The linear equation is $\Delta Rct = 583.2 + 671.11 LgCPb^{2+}$ (mol/ ($R^2 = 0.992$), and the LOD is 0.38 nmol/L.

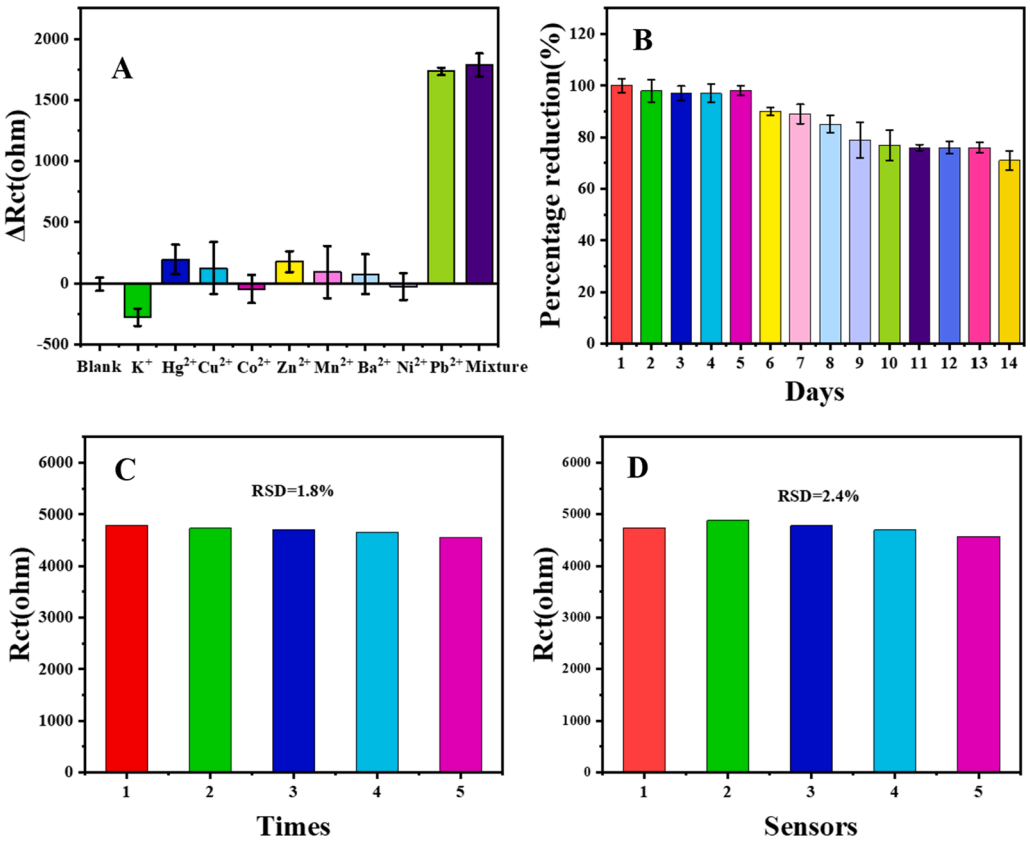

Fig. 6. Specificity (A), stability (B), repeatability (C) and reproducibility (D) of the aptamer sensor. (C^{2+}_{Pb}=50 nmol/L, other metal ions concentration is 5 μmol/L. Mixture of the eight metal ions).

Table 1
Comparison with other published methods for Pb^{2+} detection.

Methods	Signal amplification strategy	Linear range (nmol/L)	LOD (nmol/L)	Ref.
Colorimetric	DNAzyme, HCR	2.58–18	0.77	[39]
Fluorescence	UCNPs, MNPs, GNPs	25–1400	5.7	[40]
Fluorescence	–	0–1000	0.76	[41]
Electrochemical	CNTs	3.03–303030	1.18	[42]
Electrochemical	Au@Py	1.52–75.76	1.82	[15]
Electrochemical	AuNPs-GO, DNAzyme	5–1000	1	[43]
Electrochemical	PPy NPs	100–50000	55	[44]
Impedance electrochemical	SMNTs	0.3–100	0.1	[45]
Impedance electrochemical	SMNTs	1–10	0.41	[46]
Impedance Electrochemical	Au NFs, Y-DNA, HCR	0.5–1000	0.38	This work

fluorescence intensity detected by the sensor remained above 80 % after 7 days of storage, and remained above 70 % even after 14 days of storage at 4 °C (Fig. 6**B**). It can be shown that the performance of the sensing device in this experiment is relatively stable.

The repeatability and reproducibility of the sensors were evaluated by measuring the detection of 500 nmol/L Pb^{2+} by one sensor six times and six independent identical sensors, respectively, under the same detection conditions. The RSD of the detection results was low, 1.8 % (Fig. 6**C**) and 2.4 % (Fig. 6**D**), respectively, indicating that the aptamer has good repeatability and reproducibility.

To demonstrate the superiority of this sensor, a comparison is made in Table 1, which shows that the designed sensor has a wider linear range and lower detection limit compared with other Pb^{2+} detection methods. The results show that gold nanoflowers can effectively improve the sensitivity of the sensor. Therefore, electrochemical sensors have potential applications in sensitive detection of Pb^{2+}.

Table 2
The analytical results obtained from actual samples using the electrochemical sensor (n = 3).

Sample	Spiked amount (nmol/L)	Detection of the amount (nmol/L)	Average recovery (%)	RSD (%)
Tap water	0	–	–	–
	0.5	0.46	92	11.3
	10.0	11.63	116.3	9.6
	100.0	101.95	110.95	3.4
tea	0	–	–	–
	0.5	0.58	116	11.5
	10.0	10.98	109.8	8.3
	100.0	101.56	101.56	5.7

3.8. Detection of actual samples

In order to study the detection ability of the impedance sensor in actual samples, tap water and tea were determined by standard addition method. Scalar pf Pb^{2+} was added at 0.5 nmol/L, 10 nmol/L, and 100

Table 3
Detection of Pb^{2+} in QC samples (n = 3).

Quality control samples	Certified values (mg/kg)	Detection value (mg/kg)	*t*
rice flour	0.064	0.058	1.60
seaweed	1.880	1.887	3.24

nmol/L, respectively. Under the optimal experimental conditions, the impedance value was measured and the recovery rate was calculated. The results are shown in Table 2. The average recoveries of tap water and tea were 92 % − 116.3 % and 101.56 % − 116 %, respectively, and the RSDs were both lower than 12 %, indicating that the sensor has potential applications in real samples. Quality control samples were also tested. (Table 3) Through *t*-test statistical analysis, at the 95 % confidence level, the calculated values of $t_{(0.95,\ n=3)}$ were all less than 4.303. It shows that the detection results of the prepared sensor are reliable.

4. Conclusion

In summary, a novel impedance electrochemical aptamer sensor was developed for sensitive detection of Pb^{2+} on bare AuE using simple modification steps. The new strategy combines dendritic DNA nanostructures with a hybrid chain reaction to increase the DNA chain loading on the electrode and reduce the difficulty of the experiment compared to the conventional DNA chain amplification method. The performance of the prepared sensor was examined under optimal experimental conditions, and it was shown that the sensor has good performance. More importantly, the prepared aptamer can accurately detect Pb^{2+} in multiple real samples with high recovery. The preparation principle and response mechanism of this work provide new insights into heavy metal detection for the environment and human health.

Translated with https://www.DeepL.com/Translator (free version).

Declaration of Competing Interest

The authors declare that they have no known competing financial interests or personal relationships that could have appeared to influence the work reported in this paper.

Data availability

I have shared the link to my data at the attach file step.

Acknowledgment

This study was funded by the Key Scientific and Technological Project of Henan Province (212102310001), The Innovative Funds Plan of Henan University of Technology (2021ZKCJ13), Science Foundation of Henan University of Technology (31401425) and Academic and technological innovation programmes for students (GJXY202215).

Appendix A. Supplementary material

Supplementary data to this article can be found online at https://doi.org/10.1016/j.bioelechem.2022.108312.

References

[1] A.L. Wani, A. Ara, J.A. Usmani, Lead toxicity: a review, Interdiscip. Toxicol. 8 (2) (2015) 55–64, https://doi.org/10.1515/intox-2015-0009.
[2] J. Xiao, R. Hu, G. Chen, Micro-nano-engineered nitrogenous bone biochar developed with a ball-milling technique for high-efficiency removal of aquatic Cd (II), Cu(II) and Pb(II), J. Hazard. Mater. 387 (2020) 121980.
[3] Y. Zhou, L. Tang, G. Zeng, C. Zhang, Y. Zhang, X. Xie, Current progress in biosensors for heavy metal ions based on DNAzymes/DNA molecules functionalized nanostructures: A review, Sens. Actuators, B. 223 (2016) 280–294, https://doi.org/10.1016/j.snb.2015.09.090.
[4] Y. Wu, Y. Shi, S. Deng, C. Wu, R. Deng, G. He, M. Zhou, K. Zhong, H. Gao, Metal-induced G-quadruplex polymorphism for ratiometric and label-free detection of lead pollution in tea, Food Chem. 343 (2020), 128425, https://doi.org/10.1016/j.foodchem.2020.128425.
[5] S. Al-Lahham, F. Rezaee, Propionic acid counteracts the inflammation of human subcutaneous adipose tissue: a new avenue for drug development, Daru. 27 (2) (2019) 645–652, https://doi.org/10.1007/s40199-019-00294-z.
[6] P. Mitra, S. Sharma, P. Purohit, P. Sharma, Clinical and molecular aspects of lead toxicity: An update, Crit Rev Clin Lab Sci. 54 (7–8) (2017) 506–528, https://doi.org/10.1080/10408363.2017.1408562.
[7] M.R. Saidur, A.R.A. Aziz, W.J. Basirun, Recent advances in DNA-based electrochemical biosensors for heavy metal ion detection: A review, Biosens. Bioelectron. 90 (2017) 125–139.
[8] B. Chen, Z. Wang, D. Hu, Q. Ma, L. Huang, C. Xv, Z. Guo, X. Jiang, Scanometric nanomolar lead (II) detection using DNA-functionalized gold nanoparticles and silver stain enhancement, Sens. Actuators, B. 200 (2014) 310–316, https://doi.org/10.1016/j.snb.2014.04.066.
[9] R. Ma, L. Wang, M. Zhang, L. Jia, W. Zhang, L. Shang, W. Jia, H. Wang, A novel one-step triggered "signal-on/off" electrochemical sensing platform for lead based on the dual-signal ratiometric output and electrode-bound DNAzyme assembly, Sens. Actuators, B. 257 (2018) 678–684, https://doi.org/10.1016/j.snb.2017.10.158.
[10] Y. Hung, T. Hsiung, Y. Chen, C. Huang, A label-free colorimetric detection of lead ions by controlling the ligand shells of gold nanoparticles, Talanta 82 (2) (2010) 516–522, https://doi.org/10.1016/j.talanta.2010.05.004.
[11] Y. Liu, Q. Guo, X. Qu, Q. Sun, Supramolecularly Assembled Ratiometric Fluorescent Sensory Nanosystem for "Traffic Light"-Type Lead Ion or pH Sensing, ACS Appl. Mater. Interfaces. 10 (36) (2018) 30662–30669, https://doi.org/10.1021/acsami.8b10007.
[12] J. Ding, D. Zhang, Y. Liu, M. Yu, X. Zhan, D. Zhang, P. Zhou, An electrochemical aptasensor for detection of lead ions using a screen-printed carbon electrode modified with Au/polypyrrole composites and toluidine blue, Anal. Methods. 11 (33) (2019) 4274–4279, https://doi.org/10.1039/c9ay01256g.
[13] J.G. Manjunatha, A surfactant enhanced graphene paste electrode as an effective electrochemical sensor for the sensitive and simultaneous determination of catechol and resorcinol, Chem. Data Collect. 25 (2020), 100331, https://doi.org/10.1016/j.cdc.2019.100331.
[14] Y. Cai, B. Ren, C. Peng, C. Zhang, X. Wei, Highly Sensitive and Selective Fluorescence "Turn-On" Detection of Pb (II) Based on Fe3O4@Au-FITC Nanocomposite, Molecules 26 (11) (2021) 3180, https://doi.org/10.3390/molecules26113180.
[15] H. Chen, R. Li, K. Wu, P. Hu, Z. Zhang, N. Huang, W. Zhang, J. Chen, Experimental and theoretical validations of a one-pot sequential sensing of Hg^{2+} and biothiols by a 3D Cu-based zwitterionic metal−organic framework, Talanta 210 (2020), 120596, https://doi.org/10.1016/j.talanta.2019.120596.
[16] Y. Liu, Y. Liu, B. Liu, A dual-signaling strategy for ultrasensitive detection of bisphenol A by aptamer-based electrochemical biosensor, J. Electroanal. Chem. 781 (2016) 265–271, https://doi.org/10.1016/j.jelechem.2016.06.048.
[17] A. Hayat, S. Andreescu, J.L. Marty, Design of PEG-aptamer two-piece macromolecules as convenient and integrated sensing platform: Application to the label free detection of small size molecules, Biosens. Bioelectron. 45 (2013) 168–173, https://doi.org/10.1016/j.bios.2013.01.059.
[18] Y. Sun, J. Zhao, L. Liang, Recent development of antibiotic detection in food and environment: The combination of sensors and nanomaterials, Microchim. Acta 188 (1) (2021) 1–22, https://doi.org/10.1007/s00604-020-04671-3.
[19] N. Xue, S. Wu, Z. Li, X. Miao, One-step and ultrasensitive ATP detection by using positively charged nano-gold@ graphene oxide as a versatile nanocomposite, Anal. Bioanal. Chem. 412 (11) (2020) 2487–2494, https://doi.org/10.1007/s00216-020-02470-6.
[20] N. Wang, Y. Han, Y. Xu, C. Gao, X. Cao, Detection of H_2O_2 at the nanomolar level by electrode modified with ultrathin AuCu Nanowires, Anal. Chem. 87 (1) (2015) 457–463, https://doi.org/10.1021/ac502682n.
[21] Y. Wang, M. Lv, Z. Chen, Z. Deng, N. Liu, J. Fan, W. Zhang, A fluorescence resonance energy transfer probe based on DNA-modified upconversion and gold nanoparticles for detection of lead ions, Front. Chem. 8 (2020) 238, https://doi.org/10.3389/fchem.2020.00238.
[22] B. He, S. Wang, An electrochemical aptasensor based on PEI-C3N4/AuNWs for determination of chloramphenicol via exonuclease-assisted signal amplification, Microchim. Acta 188 (1) (2021) 22, https://doi.org/10.1007/s00604-020-04688-8.
[23] P. Shende, P. Kasture, R.S. Gaud, Nanoflowers: The future trend of nanotechnology for multi-applications, Artif Cells Nanomed, Biotechnol. 46 (2018) S413–S422, https://doi.org/10.1080/21691401.2018.1428812.
[24] H. Cui, K. An, C. Wang, Y. Chen, S. Jia, J. Qian, N. Hao, J. Wei, K. Wang, A disposable ratiometric electrochemical aptasensor with exonuclease I-powered target recycling amplification for highly sensitive detection of aflatoxin B1, Sens. Actuators, B. 355 (2022), 131238, https://doi.org/10.1016/j.snb.2021.131238.
[25] Y. Ke, L. Ong, W. Shih, P. Yin, Three-dimensional structures self-assembled from DNA bricks, Science 338 (6111) (2012) 1177–1183, https://doi.org/10.1126/science.1227268.
[26] J. Chen, J. Wen, G. Yang, S. Zhou, A target-induced three-way G-quadruplex junction for 17 beta-estradiol monitoring with a naked-eye readout, ChemComm. 51 (62) (2015) 12373–12376, https://doi.org/10.1039/C5CC04347F.
[27] A. Zheng, J. Li, J. Wang, X. Song, G. Chen, H. Yang, Enzyme-free signal amplification in the DNAzyme sensor via target-catalyzed hairpin assembly, ChemComm. 48 (25) (2012) 3112–3114, https://doi.org/10.1039/C2CC30305A.
[28] G. Wu, Z. Xiong, S. Oh, Y. Ren, Q. Wang, L. Yang, Two-color, ultra-sensitive fluorescent strategy for ochratoxin A detection based on hybridization chain reaction and DNA tweezers, Food Chem. 356 (2021), 129663, https://doi.org/10.1016/j.foodchem.2021.129663.
[29] K. Abnous, N.M. Danesh, M. Ramezani, M. Alibolandi, M.A. Nameghi, T.S. Zavvar, S.M. Taghdisi, A novel colorimetric aptasensor for ultrasensitive detection of aflatoxin M1 based on the combination of CRISPR-Cas12a, rolling circle

amplification and catalytic activity of gold nanoparticles, Anal. Chim. Acta. 1165 (2021), 338549, https://doi.org/10.1016/j.aca.2021.338549.
[30] L. Jia, R. Zhao, L. Wang, R. Ma, W. Zhang, L. Shang, H. Wang, Aptamer based electrochemical assay for protein kinase activity by coupling hybridization chain reaction, Biosens. Bioelectron. 117 (2018) 690–695, https://doi.org/10.1016/j.bios.2018.06.067.
[31] J. Yi, Z. Liu, J. Liu, H. Liu, F. Xia, D. Tian, C. Zhou, A label-free electrochemical aptasensor based on 3D porous CS/rGO/GCE for acetamiprid residue detection, Biosens. Bioelectron. 148 (2020) 1111827, https://doi.org/10.1016/j.bios.2019.111827.
[32] J. Jiang, H. Wu, Y. Su, Y. Liang, B. Shu, C. Zhang, Electrochemical cloth-based DNA sensors (ECDSs): A new class of electrochemical gene sensors, Anal. Chem. 92 (11) (2020) 7708–7716, https://doi.org/10.1021/acs.analchem.0c00669.
[33] Y. Zhou, X. Huang, W. Zhang, Y. Ji, R. Chen, Y. Xiong, Multi-branched gold nanoflower-embedded iron porphyrin for colorimetric immunosensor, Biosens. Bioelectron. 102 (2018) 9–16, https://doi.org/10.1016/j.bios.2017.10.046.
[34] J. Shi, J. Zhu, M. Zhao, Y. Wang, P. Yang, J. He, Ultrasensitive photoelectrochemical aptasensor for lead ion detection based on sensitization effect of CdTe QDs on MoS2-CdS: Mn nanocomposites by the formation of G-quadruplex structure, Talanta 183 (2018) 237–244, https://doi.org/10.1016/j.talanta.2018.02.087.
[35] L. Hao, H. Gu, N. Duan, S. Wu, X. Ma, Y. Xia, Z. Tao, Z. Wang, An enhanced chemiluminescence resonance energy transfer aptasensor based on rolling circle amplification and WS_2 nanosheet for Staphylococcus aureus detection, Anal. Chim. Acta. 959 (2017) 83–90, https://doi.org/10.1016/j.aca.2016.12.045.
[36] J.G.K. Manjunatha, B.E. Swamy, M. Deraman, G.P. Mamatha, Simultaneous determination of ascorbic acid, dopamine and uric acid at poly (aniline blue) modified carbon paste electrode: a cyclic voltammetric study, Int. J. Pharm. Pharm. Sci. 5 (Suppl. 2) (2013) 355–361.
[37] J.G. Manjunatha, B.E.K. Swamy, G.P. Mamatha, S.S. Shankar, O. Gilbert, B. S. Sherigara, Electrochemical Response of Dopamine at Phthalic acid and Triton X-100 Modified Carbon Paste Electrode: A cyclic voltammetry study, Int. J. Electrochem. Sci. 4 (10) (2009) 1469–1478.
[38] N. Hareesh, J.G. Manjunatha, A simple and low-cost poly (DL-phenylalanine) modified carbon sensor for the improved electrochemical analysis of Riboflavin, J SCI-ADV MATER DEV. 5 (4) (2020) 502–511. https://Doi.Org/10.1016/J.Jsamd.2020.08.005.
[39] G. Yang, C. Song, Q. Shi, H. Liu, S. Li, R. Liu, S. Liu, C. Lv, Amplified colorimetric sensor for detecting radon by its daughter lead based on the free-fixed auto-assembly structure of Duplex-hemin/G-quadruplex, J. Pharm. Biomed. Anal. 159 (2018) 459–465, https://doi.org/10.1016/j.jpba.2018.07.026.
[40] M. Chen, M. Hassan, H. Li, Q. Chen, Fluorometric determination of lead(II) by using aptamer-functionalized upconversion nanoparticles and magnetite-modified gold nanoparticles, J. Sci. Microchimica Acta. 187 (2020) 1, https://doi.org/10.1007/s00604-019-4030-4.
[41] D. Yang, L. Shi, Z. Zhao, Y. Fu, H. Sun, Q. Li, Y. Tang, X. Zhang, A Lead (II) Ion Sensor Based on Selective Recognition of G-quadruplex for Ethyl-substitutive Thioflavin T, ChemistrySelect. 4 (36) (2019) 10787–10791, https://doi.org/10.1002/slct.201902277.
[42] H. Wang, Y. Liu, G. Liu, Reusable resistive aptasensor for Pb(II) based on the Pb(II)-induced despiralization of a DNA duplex and formation of a G-quadruplex, Microchim. Acta 185 (2018) 2, https://doi.org/10.1007/s00604-018-2682-0.
[43] R. Yang, T, Fang, L. Lu, Q. Ye, Highly Sensitive Detection of Pb^{2+} Based on DNAzyme/AuNPs-GO Sensor by Square-Wave Voltammetry, Chinese J. Anal. Chem. 49(2) (2021)309-317. https://doi.org/ 10.19756/j.issn.0253-3820.201231.
[44] T. Xu, H. Dai, Y. Jin, Electrochemical sensing of lead(II) by differential pulse voltammetry using conductive polypyrrole nanoparticles, Microchim. Acta 187 (1) (2020) 1, https://doi.org/10.1007/s00604-019-4027-z.
[45] X. Zhu, H.F. Xu, R.L. Lin, Z.H. Wang, B.J. Zheng, G.D. Yang,G.N. Chen, DNA concatamers-based biosensor for Pb(II) using electrochemical impedance spectroscopy. Anal. Methods. 6 (22) (2014) 8886-8889. https://doi.org/ 10.1039/c4ay01230e.
[46] Y. Lian, M. Yuan, H. Zhao, DNA Wrapped Metallic Single-walled Carbon Nanotube Sensor for Pb (II) Detection, Fuller. Nanotub. Carbon Nanostructures. 22 (5) (2012) 510-518. https://doi.org/ 10.1080/1536383X.2012.690462.